

Article

# Free Space Optics Communication for Ultra-High-Speed Train Running in Evacuated Tube

Hasan Abbas Al-Mohammed and Elias Yaacoub \*

Computer Science and Engineering Department, Faculty of Engineering, Qatar University,  
Doha P.O. Box 2713, Qatar

\* Correspondence: eliasy@ieee.org

**Abstract:** This paper develops a novel communication method for an ultra-high-speed train that runs in an evacuated tube. The proposed method significantly reduces the number of needed base stations to provide adequate coverage and data rates. Moreover, the time connectivity for each base station was enhanced considerably. The proposed method can provide improvements in terms of transmitted power and received power, either fixed or variable; this method offers a fixed or variant data rate. Moreover, the paper studies the effects of the divergence angle on transmitted and received power. Additionally, the proposed communication procedure might produce a system with a fixed data rate, such as 1.25 Gbps. It can also create a design with adaptive divergence angles (that can be altered dynamically) depending on the train distance to the base station. The results show that this method is promising for working for an ultra-high-speed train that runs in an evacuated tube. It can reduce the base stations number from 500 to less than 10 base stations with respect to the data rate and power consumption. Furthermore, a new handover method is proposed and addressed in this work.

**Keywords:** free space optics; FSO; ultra-high-speed train; evacuated tube transportation



**Citation:** Al-Mohammed, H.A.;

Yaacoub, E. Free Space Optics

Communication for

Ultra-High-Speed Train Running in  
Evacuated Tube. *Appl. Sci.* **2022**, *12*,  
8545. [https://doi.org/10.3390/  
app12178545](https://doi.org/10.3390/app12178545)

Academic Editor: Nuno Silva

Received: 16 July 2022

Accepted: 23 August 2022

Published: 26 August 2022

**Publisher's Note:** MDPI stays neutral  
with regard to jurisdictional claims in  
published maps and institutional affil-  
iations.



**Copyright:** © 2022 by the authors.  
Licensee MDPI, Basel, Switzerland.  
This article is an open access article  
distributed under the terms and  
conditions of the Creative Commons  
Attribution (CC BY) license ([https://  
creativecommons.org/licenses/by/  
4.0/](https://creativecommons.org/licenses/by/4.0/)).

## 1. Introduction

Due to the general advancements in modern economy and technology, transportation has expanded dramatically since the 1950s, leading to significant demand for ultra-high-speed trains for ground transportation, with speeds exceeding 1000 km/h [1]. However, the researchers demonstrate that when the train speed approaches 400 km/h, the resistance will be more than 80% of the overall resistance. Furthermore, in a vehicle system, aerodynamic noise is proportional to one-eighth of the power speed [2].

As a result, the higher the speed, the worse the noise pollution. Furthermore, according to the European Environmental Agency, the transport sector produced 27% of total European greenhouse gas emissions in 2016. Consequently, a new magnetically levitated ultrafast train operating along a low-pressure tube is required to reduce CO<sub>2</sub> emissions [3]. Thus, many countries have researched evacuated tube transportation (ETT), such as China and the United States [1].

Since the demand for high-speed internet connectivity is becoming increasingly important in our daily lives, providing Internet access in ETTs is one of the key incentives for railway operators to attract more passengers. However, radiofrequency wireless technologies are utilized to provide Internet access to travelers. Existing infrastructure based on radio frequency technology, such as Wi-Fi/WiMAX, can theoretically provide peak data rates of 54/75 Mbps, but in practice, data rates drop to less than 10 Mbps [4,5]; furthermore, the authors of [6] optimized a cellular access to the universal mobile telecommunications system in long-term evolution for 4G networks to cover the railways by the system cells; in [7], based on Saleh-Valenzuela and WINNER II model for 5G technology, they proposed a novel non-stationary mmWave MIMO theoretical model for high-speed train communication; also, to provide a high data rate for the train in 5G+/6G networks, in [8] the author

used unmanned aerial vehicles (UAVs)/drones for providing high data rates to mobile relays placed on top of high-speed train vehicles.

However, the ultra-high-speed train based on ETT poses several communications issues. Initially, there are ultra-fast handovers and increasing latency. In addition, the ultra-high speed will cause higher Doppler spread which will cause interchannel interference for the high mobility devices [9]. Other previous works have demonstrated high speed by using Free Space Optics (FSO) rather than RF [10]. The train's transceivers must cooperate, and there is no redundant standby equipment to support reliable communication. In the FSO scenario, the operator has to erect several base stations (BSs) to maintain line of sight contact between the train and the ground and provide seamless coverage. In general, the large number of BSs incurs high costs and, in rural areas, raises operating expenses, making it a crucial concern for railway operators [4].

Therefore, it is an important target for the researchers to minimize the number of BSs. Furthermore, traveling away from a BS's coverage area and into the coverage area of the next BS initiates a handover process, which may result in communications interruption and a considerable handover time, particularly with the ultra-high-speed train. The time connectivity for each BS will be 0.72 s, or in some cases, 0.26 s if the train is traveling at 2700 km/h [1]. The train must undergo various handovers, influencing system performance (data rate). Furthermore, the large divergence angle covering a specified track distance reduces the data rate.

So, addressing the communication issue at ultra-high speed remains a significant challenge. The authors of [1] proposed a strategy for employing FSO in ETT; the proposed model contains an optical access point fixed at the ceiling of the evacuated tube every 200 m, it works as a transceiver for optical signals communication; furthermore, two optical transceivers are installed on the train, which are located on both the front and back of the train. Hence, a 100 km distance requires 500 BSs to cover it, and the data rate is adversely affected due to the wide divergence angle used.

From the above discussion, it can be noted that the increasing expansion and sophisticated growth of high train systems necessitate the provision of high-speed Internet services, which the existing radio frequency technology cannot readily offer, due to the time of handover mechanism and shortest time connectivity, especially with the ultra-high-speed future trains that would be run in an evacuated tube. Moreover, the existing techniques that use free-space optics suffer from the high number of base stations that need to be used (high expenditures). Therefore, this work proposes a unique strategy for ultra-high-speed trains in evacuated tubes based on FSO that achieves high speed, high reliability, low latency, high data rate, and fewer base stations required. Hence, in this paper, the number of base stations is significantly reduced, and the divergence angle could be adaptive depending on the distance between the train's transceiver and the stationary BS transceiver. In addition, the power consumption will be less than the other techniques depending on the distance and the divergence angle, and thus might indeed be adaptive as well. Moreover, the data rate can be fixed at 1.25 Gbps (with reduced power consumption, and changeable divergence angle) or possibly a dynamic data rate increases more than 1.25 up to 4Tbps or more depending on the situation. Furthermore, a new handover method is proposed and addressed in this work.

The remainder of this article is structured as follows. First, the system model is presented in Section 2, where the FSO technique is proposed for ultra-high-speed trains in evacuated tubes to provide excellent dependability and low latency. The handover mechanism is discussed in Section 3. Then, simulation results are presented and analyzed in Section 4. Finally, conclusions are presented in Section 5.

## 2. System Model

The proposed scheme that is used in this paper is illustrated in Figure 1. In this paper, the laser beam propagation model follows a Gaussian distribution [11]. A train vehicle has an FSO transceiver installed on the roof in our model, and each BS on the ground has an

FSO transceiver. The model contains three stages constituting the FSO communications system: a transmitter to emit optical signals, a free-space transmission channel, and a receiver to receive the signals. To enable full-duplex FSO communications, each party (i.e., the transmitter and receiver) is often outfitted with a transceiver that serves as both a transmitter and a receiver simultaneously, following the same principle that is used in [3,4,8]. Laser diodes operating at wavelengths between 780 and 1600 nm are usually preferred as the light sources for this application because they may attain high data rates over long distances. For instance, FSO communication systems are expected to provide data rates in the range of Gigabits per second for high-speed trains [6]. In this study, we will concentrate on ground-to-train communications for simplicity. Furthermore, because the transmitter and receiver of a transceiver are mutually aligned, establishing a ground-to-train communications link also guarantees a train-to-ground link [12]. As a result, our research applies to both of them. In addition, according to the authors' investigations, the speeds for evacuated tube transportation exceed 1000 km/h [1]. Therefore, two different speeds, 1000 km/h and 2700 km/h, were considered as realistic examples addressed in the paper.

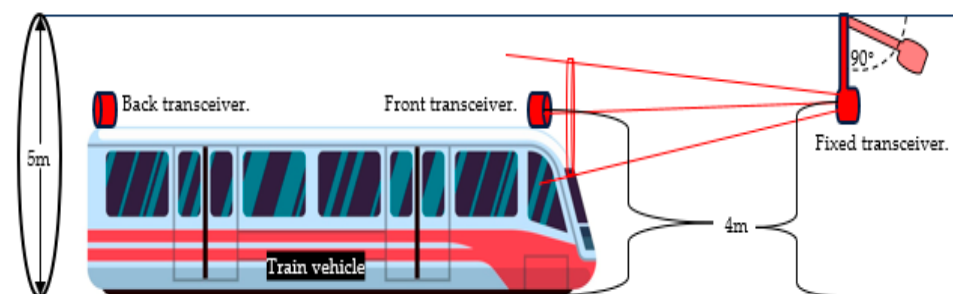


**Figure 1.** The proposed method.

The proposed technique is depicted in Figure 1. The base station is protected by a barrier on the tube's ceiling and makes a 90-degree angle with the horizontal at the maximum openness to send and receive data, while being perfectly aligned with the train's transceiver. When the train is too far away from the base station, it will fully close to make a 0-degree angle with the horizontal and enter standby mode to save power. This is the main advantage compared to other FSO techniques: The moving barrier allows perfect alignment with the transceiver on board the train, thus leading to higher data rates and longer contact time with the BS, while avoiding collision when the train reaches the BS (as it folds away while the train is at a safe distance away, after handover to another BS).

This study assumes that the train's transceiver and the BSs along the tube utilize a wavelength of 1550 nm. The 1550-nm wavelength was chosen for its availability, reliability, high-performance capabilities, and reduced cost of the transmitter and detector, as well as its suitability for eye safety [13]. In addition, the paper also considers that each BS's transceiver may be connected to a fiber-optic backbone with a wavelength of 1530 to 1565 nm (i.e., C-band) [13,14]. Although this wavelength choice allows smooth interfacing with fiber optic networks, it should be noted that different wavelengths could be used at the FSO and fiber links, with appropriate conversion carried out at the BS to relay the data over fiber using the needed wavelength.

The top view of the geometrical model of the ground-to-train FSO communications system is shown in Figure 2. In this diagram, we suppose that the train follows a track. BST is the farthest distance to the BS (BS and the train front transceiver); it is 14.2 km, considering the earth's curvature [15–17]. The vertical distance between the BS and the ground is set to 4 m (Figure 1), and it specifies the location of the shortest coverage point (C) of the beam on the track, which is 200 m away. Finally,  $\Theta$  is the laser beam's divergence angle. This angle impacts the beam radius  $w$  and the track coverage length, calculated in (1) and (2).

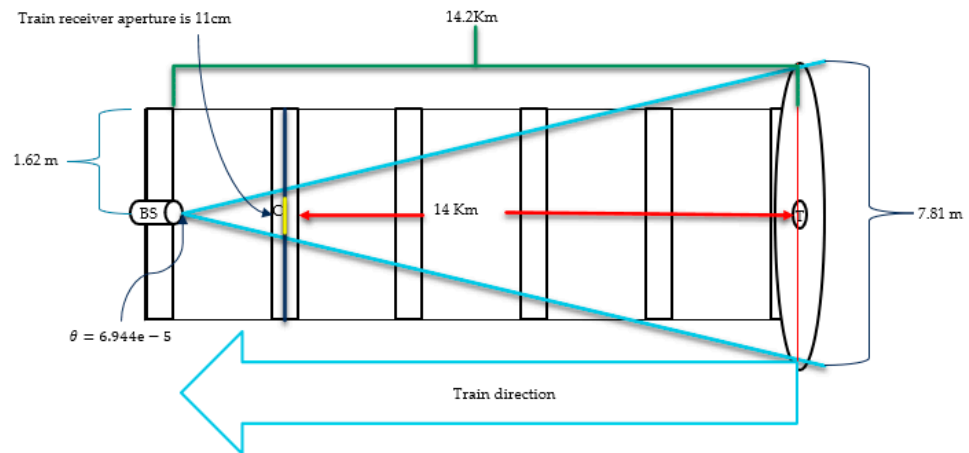


Figure 2. Top geometrical view for the proposed model (ideal case).

The radius of the beam at any distance ( $z$ ) is represented by  $w(z)$  and determined in [11]; moreover, the laser-beam propagation can be modeled by assuming that lasers generate Gaussian beams or are operating in the fundamental transverse mode (laser’s optical resonator) [18]. As a result, this paper follows this assumption and assumes that the laser beam used in this work has a Gaussian profile [19].

$$w(z) = w_0 \sqrt{1 + \left(\frac{\lambda z}{\pi w_0^2}\right)^2} \tag{1}$$

where  $z$  is the distance between the sender and the receiver,  $w_0$  is the beam waist of the laser source at the transmitter, and  $\lambda$  is the wavelength denoted as 1550 nm (Typical values of the parameters are shown in Table 1).

$$w_0 = \frac{\lambda}{\pi \theta_{1/2}} \tag{2}$$

Table 1. Evaluation parameters.

Parameter	Value
Wavelength	1550 nm
Train speed	270 m/s–750 m/s
Source diameter	5 cm
Receiver diameter	11 cm
Transmitter optical power	variable up to 1 W/cm <sup>2</sup>
Transmitter efficiency	0.9
Receiver efficiency	0.9
Beam divergence	variable
Receiver sensitivity, $P_{rs}$	−36 dBm

### 2.1. Divergence Angle

Diffraction-limited optics provide the highest laser beam narrowness, with a beamwidth of:

$$\Theta = \frac{\lambda * 2.24}{D} \tag{3}$$

where  $\lambda$  is the wavelength of laser transmission, and  $D$  is the diameter of the optical aperture of the transmitter. Considering the laser beam width that was used in [19], with a 1550 nm wavelength and the same diameter optical receiver (11 cm) as in [5], the smallest divergence angle that can work for the proposed design is  $6.944 \times 10^{-5}$  radians. By using Equation (1), the radius at the distance of 1500 m will be 5.5 cm for the angle  $6.944 \times 10^{-5}$

so this radius can cover all the transceiver lens area and acquires a high density of the beam for accurate communication.

2.2. The Received Power

The received power [20] at the receiver can be stated as follows for standard ground-to-train FSO communications:

$$P_{rx} = P_{tx} \frac{D^2}{\theta_{div}^2 L^2} 10^{-\gamma L/10} \eta_{tx} \eta_{rx} \tag{4}$$

where  $P_{tx}$  represents the transmitted power,  $\theta_{div}$  denotes transmitter divergence angle,  $D$  represents receiver diameter,  $L$  indicates communications distance,  $\gamma$  is the atmospheric attenuation coefficient in dB/km, and  $\eta_{rx}$  and  $\eta_{tx}$  denote receiver and transmitter efficiency, respectively. Since  $P_{tx}$  is 100 mW for 1 cm<sup>2</sup> and  $D$  is 11 cm [13] (e.g., see Table 1), the beam’s divergence angle (here,  $6.944 \times 10^{-5}$  is the smallest angle) is defined. The communication distance between the transmitter and receiver is determined. Therefore, the received power can be estimated with the attenuation effect.

Due to the unique design for the ETT built for air-free evacuated tubes (to mitigate the noise and the resistance of the air), the attenuation from the weather effect is zero. Therefore, instead of  $\gamma$ , we can write zero to represent it.

Or, simply Equation (5) (Friis formula) can be used instead of (4) [21]:

$$P_{rx} = P_{tx} G_{tx} G_{rx} \left( \frac{\lambda}{4\pi R} \right)^2 L_{geo} L_{tx} L_{rx} \eta_{tx} \eta_{rx} \tag{5}$$

where  $G_{tx}, G_{rx}$  correspond to the transmit and receive antenna gains,  $R$  is the communication distance between the transmitter and the receiver,  $L_{geo}$  is the geometrical loss,  $L_{tx}, L_{rx}$  are transmitter pointing loss and receiver indicating loss, respectively, and  $\eta_{tx}, \eta_{rx}$  are transmitter and receiver optical efficiency, respectively. Equation (6) gives an approximation of the transmitter antenna gain for a Gaussian beam:

$$G_{tx} = \frac{32}{\theta^2} \tag{6}$$

The receiver antenna gain is given by [21,22]:

$$G_{rx} = \left( \frac{\pi D_{rx}}{\lambda} \right)^2 \tag{7}$$

In addition,  $L_{geo}$  is given by [23]:

$$L_{geo} = \left( \frac{D_{rx}}{D_{tx} + \theta R} \right)^2 \tag{8}$$

$L_{tx}$  and  $L_{rx}$  in (4) are the transmitter and receiver pointing loss [24], respectively, which are given by:

$$L_{tx} = e^{-G_{tx} \gamma^2} \tag{9}$$

$$L_{rx} = e^{-G_{rx} \zeta^2} \tag{10}$$

where  $\gamma$  and  $\zeta$  indicate the radial aiming errors of the transmitter and receiver, respectively. Moreover, such a model should indicate the loss attenuation using Equation (11). In this paper’s case, because of the evacuated tube, there is no attenuation loss from the air fog, etc.

$$L_a = \frac{17}{V} \left( \frac{\lambda}{0.55 \mu m} \right)^{-q(\lambda)} \tag{11}$$

In (11),  $L_a$  is in dB/km,  $V$  is the weather visibility in km, and  $q$  is the size distribution of the scattering particles,  $q$  values are given in [25].

### 2.3. Data Rate

To estimate the data rate for FSO,  $P_{tx}$  the transmitted power,  $\theta$  divergence angle, receiver area  $A$ , and  $\tau_{opt}$  optical efficiency for the transmitter and receiver must be determined; thus,  $R$ , the data rate is achieved by:

$$R = \frac{P_{tx} \tau_{opt} \tau_{ATM} A}{\pi \left(\frac{\theta}{2}\right)^2 L^2 E_p N_p} \tag{12}$$

where  $E_p = \frac{hc}{\lambda}$  is the photon energy, and  $N_p$  is the receiver sensitivity in  $\frac{\text{photons}}{\text{bit}}$ .

Furthermore, power at the receiver  $P_{REQ}$  (watts) to achieve a given data rate,  $R$  (bits/sec), is given by  $P_{REQ}$  [21]:

$$P_{REQ} = N_p R h \nu = \frac{N_p R h c}{\lambda} \tag{13}$$

where  $\nu$  is the frequency of the laser light ( $h = \text{Planck's constant}$ ,  $c$  is the velocity of light). However, In Si and InGaAs avalanche photodetectors, the usual receiver sensitivity for transmitting at 1.25 Gbps with ON-OFF keying modulation is  $-36$  dBm, as it was calculated by previous researchers in real-world scenarios [23], and this paper uses the same metrics and equations for calculated the received power (dBm), and it took as a reference the works in [10,26]. Therefore, the work in this paper and all assumptions focus on this sensitivity, considering the different received power calculated for several divergence angles and distances.

### 3. Handover Mechanism

First of all, in the system's initial state, there are two controllers in the proposed system (method) to do the handover mechanism to keep the train connected to the internet.

The first controller manages the networking of the train's track, such as the communication of the BSs, sensors, and the backbone network [5,27]. The second controller is located inside the train and used for managing the networking and the communication inside the train vehicles.

Furthermore, all base stations are in standby mode for power consumption. Therefore, they stand fully closed (the barrier that carries the transceiver is 0 degrees with the horizontal and 90 degrees with the train receiver), indicating that the bars (the BS's holder) are still not moving to wait for the signal, see Figure 3. In addition, sensors are placed along the track to assess train position for network purposes and other objectives.

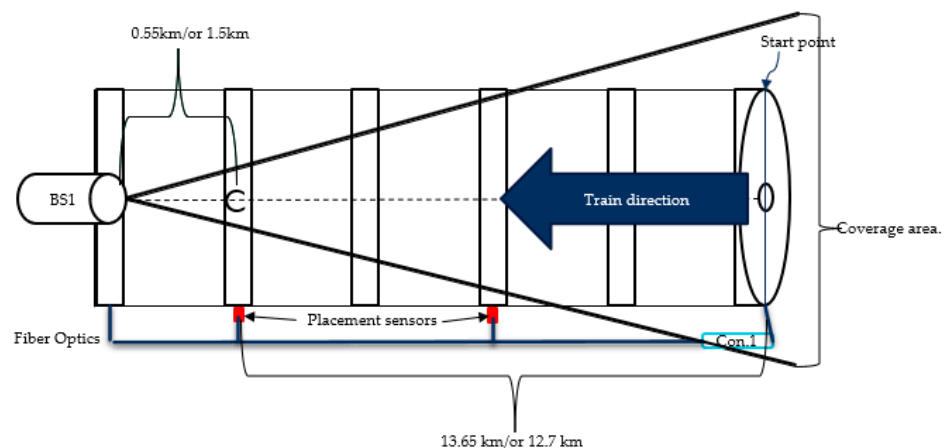


Figure 3. The initial state of the handover mechanism.

Moreover, each transceiver communicates with the outside network by considering that the transceiver of each BS might be connected to a fiber-optic backbone, where a wavelength between 1530 and 1565 nm (i.e., C-band) is usually employed [13,14].

For an ultra-speed train traveling at 1000 km/h, the distance between the barrier (BS) and the closest point (C) that the BS can cover and communicate with is 0.55 km (the train's speed is 1000 km/h which means 277 m/s, and the barrier needs 2 s to close, the distance reached by the train will be  $277\text{ m} + 277\text{ m} = 0.55\text{ km}$ ), and the bar may be entirely closed without being disturbed by the train; the barrier requires 2 s to fully close [28,29], and if the train is traveling at 2700 km/h, the nearest point will be 1.5 km (the train's speed is 2700 km/h which means 750 m/s, and the barrier needs 2 s to close, the distance reached by the train will be  $750\text{ m} + 750\text{ m} = 1.5\text{ km}$ ). Moreover, these distance measurements impact the divergence angle that should be employed, transmitted power, and the data rate and BS coverage range.

BS1 maintains communication with the front train until the train reaches the C point, at which point the controller sends a control signal to BS2 to open the barrier fully. Once the bar (BS's holder) opens communication with the transceiver at the back of the train, when controller 2 receives a signal from the transceiver at the back of the train, it sends a control signal to the front transceiver. However, at a distance of 0.55 km or 1.5 km (depending on train speed), this space allows barrier 1 to open and connect with the train's transceiver fully, see Figure 4. Figure 5 provides an overview of the handover process.

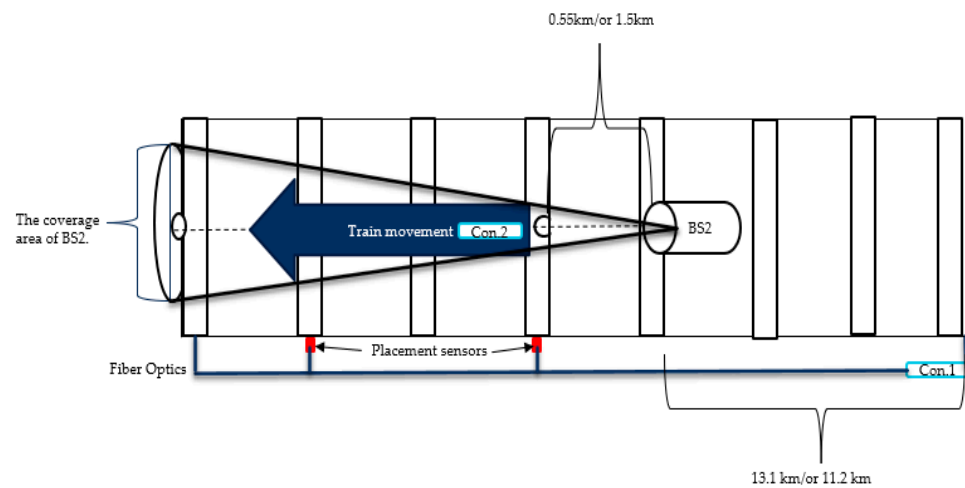


Figure 4. BS2 handover mechanism.

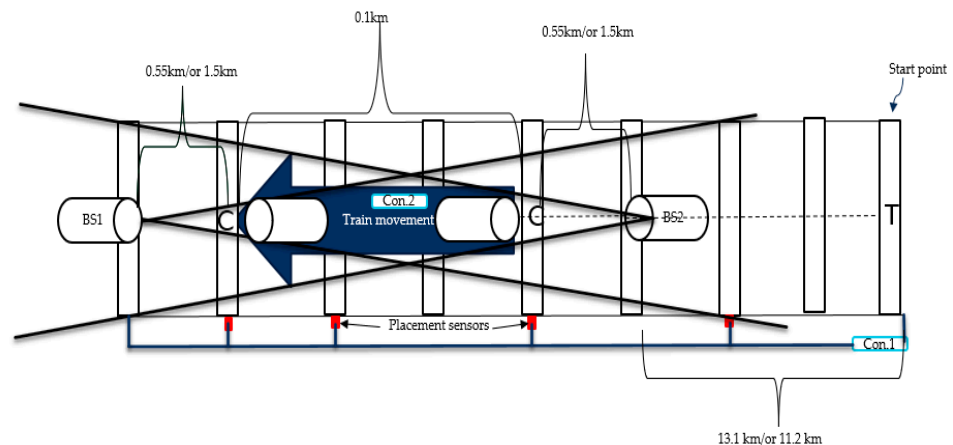
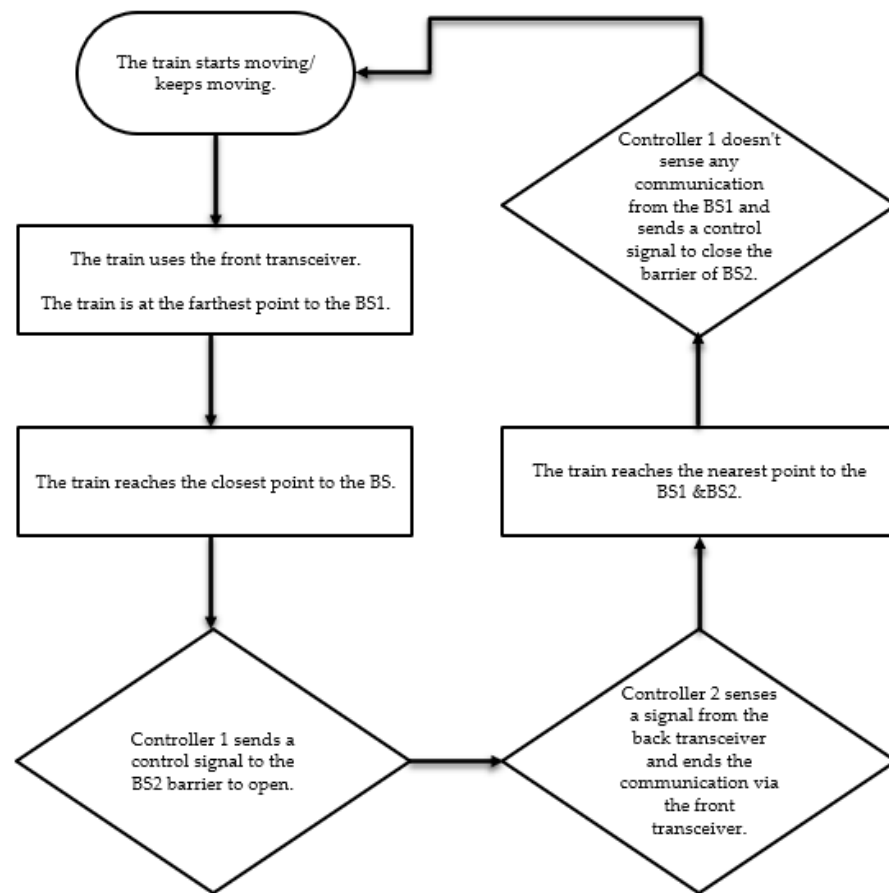


Figure 5. Overview of the handover mechanism.

When BS2 does not receive any laser beam from the front train transceiver, the barrier of BS2 does close and turn to standby mode waiting for the next train coming. These procedures continue for the next BSs all along the track until the train reaches the destination.

Moreover, Figure 6 shows a flowchart of the process of the system to do the handover.



**Figure 6.** Flow chart of the handover process.

For a train speed of 1000 km/h, the coverage distance of BS1 will be as follows: uncovered area BS1C is 550 m, this is the nearest point to the BS which is (C), when the train front transceiver is at that point; the same distance will not be covered by BS2 when BS1 needs to be closed or at the nearest point (C, 2 s closing procedure). In addition, the train length should be considered as it affects the final length, which is assumed to be a 100 m train. Therefore, uncovered area will be  $|BS1C| + |BS2C| + \text{train length}$ , and equals 1200 m. This distance should be subtracted from the total area between BS1 and the start point  $|BS1T|$ , which is 14.2 km, so, the BS for speed 1000 km/h actually covers a distance of 13 km.

On the other hand, if the train speed is 2700 km/h, the coverage distance for BS1 will be: uncovered area BS1C is 1500 m, this is the nearest point to the BS which is (C), when the train front transceiver is at that point; the same distance will not be covered by BS2 when BS1 needs to be closed or at the closest point (C, 2 s closing procedure). In addition, the train length should not be considered as it affects the final length, which is assumed to be a 100 m train. Therefore, uncovered area will be  $|BS1C| + |BS2C| + \text{train length}$ , and equals 3.1 km. This distance should be subtracted from the total area between BS1 and the start point  $|BS1T|$ , which is 14.2 km, so, the BS for speed 2700 km/h actually covers a distance of 11.1 km. Compared with the scenario of [1], this is a significant improvement as the base station in [1] covered 200 m, and therefore, the distance between a BS and the next one was 200 m in [1].

## 4. Results and Discussion

This section discusses the proposed model results and the effects of the divergence angle on the data rate, received power, distance, and the impact of fixed transmitted power and divergence angle on the received power. This section will attempt to calculate the effect of different train speeds, e.g., 1000 km/h and 2700 km/h. It should be noted that this study was implemented by using MATLAB®.

### 4.1. Simulation Results

#### 4.1.1. Divergence Angle

This section attempts to answer two questions: which divergence angle does have the closest zone to the BS (a dead zone that cannot cover the transceiver with the required divergence radius)? Furthermore, what effect will employing fixed and adaptive beam radius variation with train speed have on received and transmitted power; how will they affect distance along the track (tube)?

To ensure receiving sufficient power, the nearest point to the BS should have a divergence radius equal to the radius of the transceiver (e.g., dimensions shown in Table 1), to ensure adequate reception. Therefore, Equations (1) and (2) will be used to generate the analysis data.

Figure 7 shows that the smallest divergence angle that can be used for the proposed design is  $6.944 \times 10^{-5}$  rad. The distance of 550 m with this angle gives 0.05 m divergence at the nearest point between the sender and the transmitter. We cannot use this angle to achieve the requirements of Table 1 (where the beam should cover the receiver diameter of 11 cm), unless the barrier will change the angle and end the transmission at a distance of 1.5 km. Hence, in this case, a higher number of base stations will be required and the time connectivity with each BS will be less compared to other larger divergence angles.

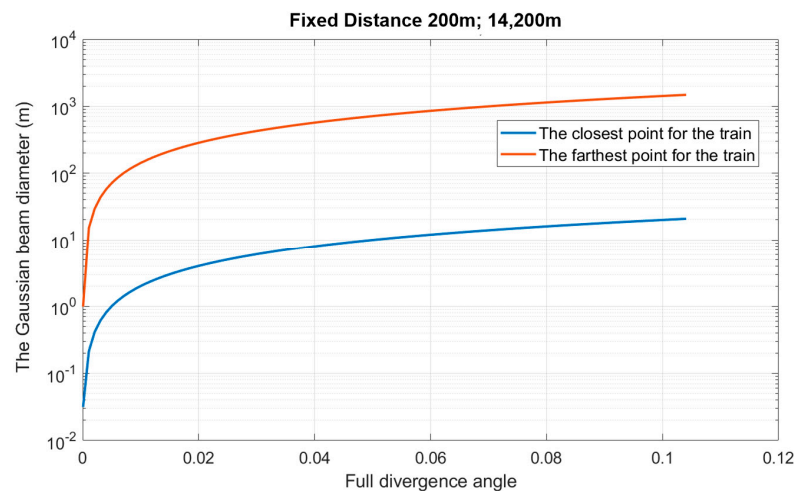


**Figure 7.** Gaussian beam diameter versus divergence angles for the proposed method.

Figure 8 represents the Gaussian beam distribution diameter for the smallest angle that can be used for the proposed system ( $6.944 \times 10^{-5}$ ); starting at a distance of 550 m, this distance required for the train speed of 1000 km/h to pass the space to reach the base station in 2 s; at this point (at a distance of 550 m), the diameter of the laser beam is 5 cm, it cannot cover the receiver's aperture in the scenario of Table 1, as it should be 11 cm.

Furthermore, the figure depicts the diameter at a distance of 1500 (required for the train to cross in 2 s) as 11 cm, so it is appropriate when the train speed is 2700 km/h. In this work, the two scenarios will be analyzed and discussed.

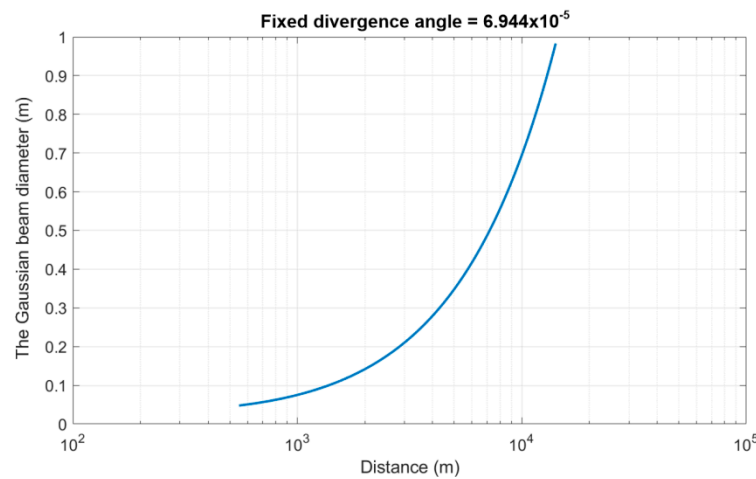


**Figure 8.** Gaussian beam diameter versus distance for a fixed divergence angle.

Table 2 indicates the distance of the chosen position for the fixed divergence angle, and it is evident that the angle ( $6.944 \times 10^{-5}$ ) is appropriate for a length of 1500 m, as well as the diameter of the farthest point (14,200 m) to be one meter (according to the values Table 1, where the beam divergence should cover at least the receiver diameter of 11 cm).

**Table 2.** Variable distance and beam divergence for fixed divergence angle  $6.944 \times 10^{-5}$ .

Distance (m)	Divergence Beam Diameter (m)
550	0.0504
1400	0.101
1500	0.11
14,200	1

The distance of the chosen position for the set divergence angles is shown in Table 3. It is clear that the angle ( $2.0944 \times 10^{-4}$ ) is adequate for a distance of 550 m since the diameter of the Gaussian beam is 11 cm, which is enough to cover the receiver’s aperture, and the diameter of Gaussian distribution for the farthest distance is 2.97 m.

**Table 3.** Variable divergence angles and beam diameter for a fixed distance of 550 m.

Full Divergence Angle	Divergence Beam Diameter (m)
$6.944 \times 10^{-5}$	0.047
$2.0944 \times 10^{-4}$	0.11
$2.4944 \times 10^{-4}$	0.13

#### 4.1.2. The Received Power

The received power is undoubtedly affected by the transmitted power, impacting the data rate. Furthermore, according to Equations (4) and (5), the received power directly influences the required transmitted power; therefore, a fixed received power ensures the desired data rate, such as 1.25 Gbps for example. The received power will be  $-36$  dBm and can employ a variety of transmitted power, which will affect the power consumption of each base station and transceiver on the train and the overall system power consumption.

Furthermore, fluctuations in transmitted power with fixed needed received power (leading to a constant data rate) can vary the system design by employing an adaptive system based on the distance between the transmitter and the receiver.

Figure 9 represents three places on the train track: 550 m is the last point covered by the BS for train speeds of 1000 km/h, 1500 m is the end covered position by the BS for train speeds of 2700 km/h, and 14,200 m is the first and farthest point from the BS. In addition,

the figure depicts several divergence angles for each position to compare the influence of the divergence angle on the transmitted power for the data rate of 1.25 Gbps, the whole angle ranging from  $6.944 \times 10^{-5}$  to 0.0523 rad [30].

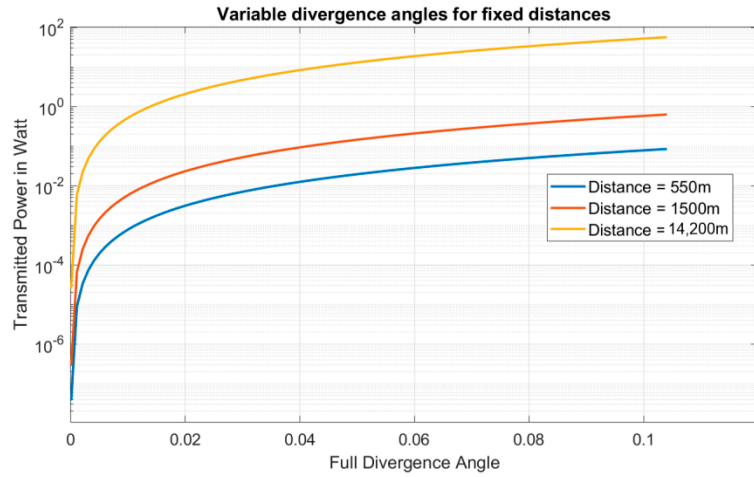


**Figure 9.** Transmit power versus divergence angle for several fixed distances: (a) distance of 550 m, (b) distance of 1500 m, (c) distance of 14,200 m.

The divergence angle affects the transmitted power, which is less in narrow angles compared to wide divergence angles. Furthermore, the same angle varies with distance, and it is clear from the figure that the close points to the BS require less power than the far points to the BS, as expected, in order to achieve the target data rate.

Figure 10 displays two divergence angles employed in the proposed system ( $6.944 \times 10^{-5}$  and  $2.0944 \times 10^{-4}$  rad), with distance changes and effects on transmitted power (dBm). Furthermore, Table 4 reveals that at 550 m, the transmitted power is  $1.7 \times 10^{-9}$  W, while at 14,200 m, the transmitted power is  $1.2 \times 10^{-4}$  W for an angle of  $6.944 \times 10^{-5}$ , yielding a fixed received power of  $-36$  dBm and a data rate of 1.25 Gbps.

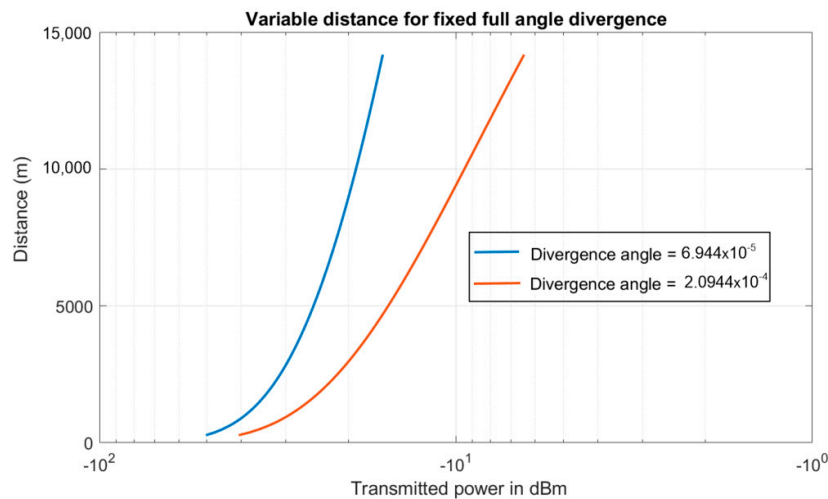


**Figure 10.** Distance versus transmitted power required for fixed data rate 1.25 Gbps.

According to the authors’ investigations, the system that was used in ultra-high-speed trains in ETT [1] did not present results for the transmitted or received power. Hence, we found results for the transmitted power that was used in the FSO systems for a train to ground BSs only in high-speed trains; therefore, this paragraph describes and compares the paper results with works that used FSO in the high-speed train scenario, and that used

transmitted power equal to 27 mW [10,26]. Thus, Figure 11 shows the received power (8) for a fixed transmit power of 27 mW.

**Table 4.** Transmitted power required for 1.25 Gbps and variable distance with two types of divergence angles.

Full Divergence Angle	Distance (m)	Transmitted Power in Watt
$6.944 \times 10^{-5}$	550	$1.764 \times 10^{-9}$
	1500	$2.5 \times 10^{-7}$
	14,200	$1.2 \times 10^{-4}$
$2.0944 \times 10^{-4}$	550	$2.165 \times 10^{-7}$
	1500	$1.2 \times 10^{-5}$
	14,200	$6.54 \times 10^{-4}$



**Figure 11.** Received power versus variable distance for two divergence angles (assuming a transmit power  $P_{tx} = 27$  mW).

The distance close to the BS has the highest received power, as expected, when the transmit power is fixed. The value decreases when the distance increases, but remains more than the  $-36$  dBm level (Table 1) needed to acquire 1.25 Gbps; so the results are good enough to maintain a high data rate for the passenger and make it possible to run live stream programs. For example, in Table 5, for the smallest divergence angle at a distance of 1500 m, the received power is 4.2 dBm while at the same length for the angle  $2.0944 \times 10^{-4}$  the power is 2.1 dBm, and so on (see Table 5).

**Table 5.** The received power for variable distance with two types of divergence angles ( $P_{tx} = 27$  mW).

Full Divergence Angle	Distance (m)	Received Power in dBm
$6.944 \times 10^{-5}$	1500	4.2
	14,200	-5.5
$2.0944 \times 10^{-4}$	550	4.2
	14,200	-17.5

Since the train operates within ETT and all of the train is covered with material (the laser cannot pass through it), and there is no glass, so, there are no effects of the laser beam on the eyes safety; therefore, it is possible to increase the power to more than 100 mW per  $\text{cm}^2$ . Figure 12 shows the received power in dBm calculated with a fixed transmitter power of 1 watt and two divergence angles.



**Figure 12.** Received power versus distance for two values of the divergence angle (assuming a transmit power  $P_{tx} = 1$  W).

Table 6 displays some of these values. The results are significantly enhanced compared to those obtained with a transmit power of 27 mW. The results were generated for both angles ( $6.944 \times 10^{-5}$  and  $2.0944 \times 10^{-4}$ ).

**Table 6.** The received power for variable distance with two types of divergence angles ( $P_{tx} = 1$  W).

Full Divergence Angle	Distance(m)	Received Power in dBm
$6.944 \times 10^{-5}$	1500	20
	14,200	10
$2.0944 \times 10^{-4}$	550	20
	14,200	-2.1

#### 4.1.3. Data Rate

The data rate is calculated by using Equations (13) and (14). In the theoretical values displayed in Figure 13, the transmitted power is 27 mW as indicated before, and the data rate for the nearest point to the BS with narrow divergence angle indicates to be more than 4Tbps. In contrast, the wide divergence angle in the figure shows a high data rate of more than 500 Gbps. Moreover, the data rate results showed the advantage of using narrow angles instead of wide angles.

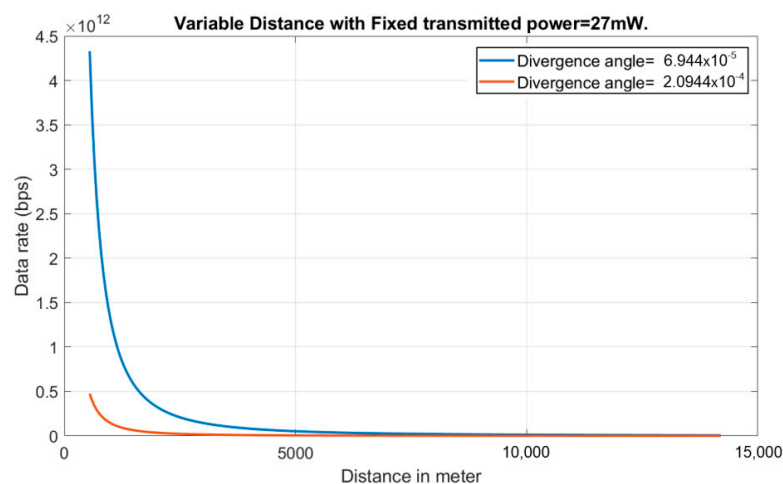


**Figure 13.** Data rate versus distance for two values of the divergence angle.

Finally, Figures 14 and 15 are utilized to describe the actual contribution of the suggested method in terms of time connectivity and the number of BSs employed in the systems compared to other works in the literature.

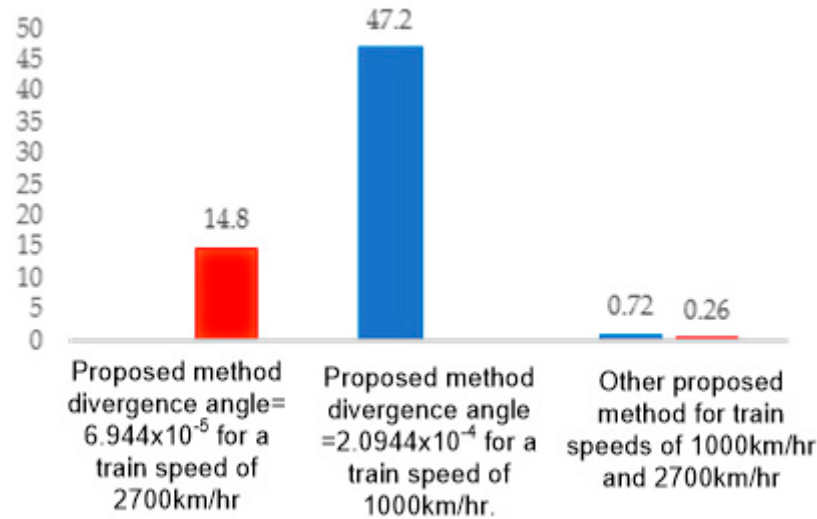


Figure 14. The time connectivity for the proposed method with others.

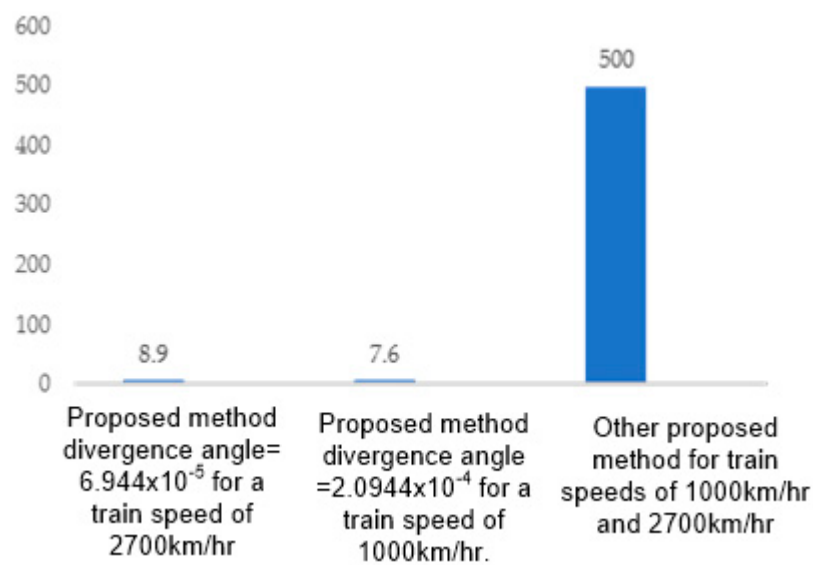


Figure 15. The number of base stations required for 100 km.

Figure 14 illustrates the time connectivity for the proposed method (i.e., the time the train remains successfully connected to a BS), including the two train speeds, 1000 km/h and 2700 km/h. Additionally, the figure compares the results to those of [1], who also used FSO in an ultra-high-speed train. The other methods in the literature designed FSO’s BSs only for a high-speed train (the train speed up to 400 km/h, not ETT). The best results in these works have a time connectivity for each BS of 2.8 s and 1.06 s [5].

The red bars in the figure indicate the train speed of 2700 km/h, and the blue bars represent the train speed of 1000 km/h. The figure also shows that the time connectivity for the other approach is 0.72 s for the train speed of 1000 km/h. While the proposed method has a time connectivity of more than 47 s, the time connectivity to the compared approach [1] is 0.26 s at a speed of 2700 km per hour. However, the proposed technique indicates 14.8 s for each BS, which affects favorably the frequency of the handover mechanism.

Figure 15 shows the number of BSs required to provide coverage for each 100 km; additionally, the figure includes a comparison with the method of [1], which is used in

an ultra-high-speed train, because the other methods (as with the time connectivity case) designed FSO's BSs only for a high-speed train (the train speed up to 400 km/h), where the best results show that 125 BSs are used for 100 km [5].

The figure also demonstrates that the other strategy [1] requires 500 BSs at any speed. At the same time, the proposed technique has less than 9 BSs at a train speed of 2700 km/h, and fewer than 8 BSs for a train speed of 1000 km/h.

These results are optimistic regarding time connectivity or reducing the number of BSs necessary for design, while maintaining the maximum data rate.

#### 4.2. Discussion of Some Practical Limitations

In this section, we discuss some practical challenges faced by the proposed ETT approach along with potential methods of overcoming them.

In this paper, we considered the diameter of the Gaussian beam limiting signal strength. Additional concerns such as alignment and focus could also be significant factors. However, given that the ETT is running by using the magnetic field, the impact of vibration should be less severe than in traditional trains. Nevertheless, to the best of the authors' knowledge, most relevant publications assume ideal conditions and no research discussing in detail the vibration issue in ETT has been found. Thus, this is a topic worthy of further investigation. In [1], the authors suggested the use of a Powell lens to expand the beam, which allows dealing with the difficulty of detection in the case of vibration. With this approach, the energy would be concentrated over a line, as opposed to a central focus in the case of a Gaussian beam profile, where the energy is reduced as we move from the center. This solution can be applied to our scenario, although in our case the presence of a moving barrier to align the beam (instead of having the transmitter at the side of the track or above the train as in the literature), could also benefit from other techniques. For example, a potential solution could be the use of a feedback control system with servo motor in order to maintain alignment. Given the high achievable data rates with FSO, the amount of data needed for feedback would be negligible and would not disrupt user data communications.

Another issue worthy of further investigation is the use of shorter wavelengths to reduce beam divergence, which would also increase the received power and the data rate as well. However, this should be carried out while taking into account the characteristics of the laser transmitter and receiver, and especially safety issues: In fact, the wavelength should be suitable with the sender angle to make the laser safe to use in any area, and to ensure there is no effect on the human eyes, according to the International Electrotechnical Commission (IEC) guidelines [31].

Finally, we comment on the issue of the curvature of the earth and maintaining line of sight, which affects the number of base stations. The curvature problem could be overcome by installing a system of mirrors for example; however, these should be carefully aligned and maintained to relay the signal properly, and would pose an additional maintenance overhead. Moreover, they would be installed on the side of the track and cannot be perfectly aligned with the receiver which would not lead to significant distance extension, as is the case when using the moving barrier of Figure 1, unless a mirror will also be carried by a moving barrier.

## 5. Conclusions

This study developed a new communication system for an ultra-high-speed train running in an evacuated tube. The proposed work was compared to existing schemes to demonstrate its capabilities, and it was applied for two types of train speeds (1000 km/h and 2700 km/h).

The proposed method can use a fixed angle depending on the train's speed or an adaptive angle, and the divergence angle can change before 1500 m; the base station could be used with an angle of  $6.994 \times 10^{-5}$  rad (to acquire the advantage of high data rate, small transmitted power) at the start of the transmission, then change to angle of  $2.0944 \times 10^{-4}$  rad at 1500 m (when the train's transceiver reaches this distance) to acquire

the required divergence radius. In addition, we can design a system with adaptive transmitted power that can change depending on the train distance to the BS with respect to the data rate for instance 1.25 Gbps power consumption.

Compared to other techniques, the results showed that the proposed approach with moving barrier holding the BS leads to a significantly lower number of required BSs (and thus significantly less handovers and longer contact time with each BS), while achieving significantly higher data rates, or requiring significantly less power to achieve the same target rate.

**Author Contributions:** Conceptualization, H.A.A.-M. and E.Y.; methodology, H.A.A.-M. and E.Y.; software, H.A.A.-M.; validation, H.A.A.-M.; investigation, H.A.A.-M. and E.Y.; resources, H.A.A.-M. and E.Y.; writing—original draft preparation, H.A.A.-M.; writing—review and editing, E.Y.; visualization, H.A.A.-M. and E.Y.; supervision, E.Y.; project administration, E.Y.; funding acquisition, E.Y. All authors have read and agreed to the published version of the manuscript.

**Funding:** This publication was jointly supported by Qatar University and IS-Wireless—IRCC Grant no. IRCC-2021-003. The findings achieved herein are solely the responsibility of the authors.

**Acknowledgments:** The authors want to thank the Editor and the Reviewers for their comments that helped enhance the quality and clarity of this paper. This publication was jointly supported by Qatar University and IS-Wireless—IRCC Grant no. IRCC-2021-003. The findings achieved herein are solely the responsibility of the authors.

**Conflicts of Interest:** The authors declare no conflict of interest.

## References

- Huang, X.; Yang, F.; Song, J.; Han, Z. An Optical Communication Approach for Ultra-High-Speed Train Running in Evacuated Tube: Potentials and Challenges. *IEEE Wirel. Commun.* **2021**, *28*, 70–76. [CrossRef]
- Safaei, F.; Suratgar, A.A.; Afshar, A.; Mirsalim, M. Characteristics Optimization of the Maglev Train Hybrid Suspension System Using Genetic Algorithm. *IEEE Trans. Energy Convers.* **2015**, *30*, 1163–1170. [CrossRef]
- Lafoz, M.; Navarro, G.; Torres, J.; Santiago, Á.; Nájera, J.; Santos-Herran, M.; Blanco, M. Power supply solution for ultrahigh speed hyperloop trains. *Smart Cities* **2020**, *3*, 642–656. [CrossRef]
- Fan, Q.; Taheri, M.; Ansari, N.; Feng, J.; Rojas-Cessa, R.; Zhou, M.; Zhang, T. Reducing the Impact of Handovers in Ground-to-Train Free Space Optical Communications. *IEEE Trans. Veh. Technol.* **2018**, *67*, 1292–1301. [CrossRef]
- Fan, Q.; Ansari, N.; Feng, J.; Rojas-Cessa, R.; Zhou, M.C.; Zhang, T. Reducing the number of FSO base stations with dual transceivers for next-generation ground-to-train communications. *IEEE Trans. Veh. Technol.* **2018**, *67*, 11143–11153. [CrossRef]
- Micheli, D.; Barazzetta, M.; Diamanti, R.; Obino, P.; Lattanzi, R.; Bastianelli, L.; Primiani, V.M.; Moglie, F. Over-The-air tests of high-speed moving LTE users in a reverberation chamber. *IEEE Trans. Veh. Technol.* **2018**, *67*, 4340–4349. [CrossRef]
- Liu, Y.; Wang, C.X.; Huang, J.; Sun, J.; Zhang, W. Novel 3-D Nonstationary MmWave Massive MIMO Channel Models for 5G High-Speed Train Wireless Communications. *IEEE Trans. Veh. Technol.* **2019**, *68*, 2077–2086. [CrossRef]
- Yaacoub, E. Ad Hoc Networks Travel Hopping Enabled Resource Allocation (THEResA) and delay tolerant networking through the use of UAVs in railroad networks. *Ad Hoc Netw.* **2021**, *122*, 102628. [CrossRef]
- Liu, J.; Wang, X. Handover Analysis on High Speed Train with Doppler Frequency Spread. 2017. Available online: <http://arxiv.org/abs/1703.09869> (accessed on 9 June 2022).
- Fathi-Kazerooni, S.; Kaymak, Y.; Rojas-Cessa, R.; Feng, J.; Ansari, N.; Zhou, M.; Zhang, T. Optimal Positioning of Ground Base Stations in Free-Space Optical Communications for High-Speed Trains. *IEEE Trans. Intell. Transp. Syst.* **2018**, *19*, 1940–1949. [CrossRef]
- Goldsmith, P.F. *Quasioptical Systems Gaussian Beam Quasioptical Propagation and Applications*; Wiley: New York, NY, USA, 1998.
- Urabe, H. High data rate ground-to-train free-space optical communication system. *Opt. Eng.* **2012**, *51*, 031204. [CrossRef]
- Paudel, R.; Ghassemlooy, Z.; Le-Minh, H.; Rajbhandari, S. Modelling of free space optical link for ground-to-train communications using a Gaussian source. *IET Optoelectron.* **2013**, *7*, 1–8. [CrossRef]
- Killinger, D. Free Space Optics for Laser Communication Through the Air. *Opt. Photonics News* **2002**, *13*, 36. [CrossRef]
- Doerry, A.W. Earth Curvature and Atmospheric Refraction Effects on Radar Signal Propagation. 2013. Available online: <http://prod.sandia.gov/techlib/access-control.cgi/2012/1210690.pdf> (accessed on 9 June 2022).
- He, X.; Stammes, K.; Bai, Y.; Li, W.; Wang, D. Effects of Earth curvature on atmospheric correction for ocean color remote sensing. *Remote Sens. Environ.* **2018**, *209*, 118–133. [CrossRef]
- Sun, W.; Okubo, S. Effects of earth's spherical curvature and radial heterogeneity in dislocation studies—for a point dislocation. *Geophys. Res. Lett.* **2002**, *29*, 46-1–46-4. [CrossRef]
- Larry, R.L.P.; Andrews, C. *Laser Beam Propagation through Random Media*, 2nd ed.; Society of Photo-Optical Instrumentation Engineers (SPIE) Press: Bellingham, WA, USA, 2005. [CrossRef]

19. Aviv, D.G. *Laser Space Communications*; Artech House: Boston, MA, USA, 2006.
20. Muhammad, S.S. Characterization of fog attenuation in terrestrial free space optical links. *Opt. Eng.* **2007**, *46*, 066001. [[CrossRef](#)]
21. Bjarklev, B.A.; Lyngby, D.; Chowdhury, C.; Majumdar, A.; Hills, A.; Nakasawa, M.; Someda, S.C.G.; Padova, H.-G. *Weber, Free-Space Laser Communications: Principles and Advances*; Springer Science & Business Media: Berlin, Germany, 2008.
22. Henniger, H.; Wilfert, O. An introduction to free-space optical communications. *Radioengineering* **2010**, *19*, 203–212.
23. Bloom, S.; Korevaar, E.; Schuster, J.; Willebrand, H. Understanding the performance of free-space optics [Invited]. *J. Opt. Netw.* **2003**, *2*, 178. [[CrossRef](#)]
24. Liu, X. Free-space optics optimization models for building sway and atmospheric interference using variable wavelength. *IEEE Trans. Commun.* **2009**, *57*, 492–498. [[CrossRef](#)]
25. Kim, I.I.; McArthur, B.; Korevaar, E.J. Comparison of laser beam propagation at 785 nm and 1550 nm in fog and haze for optical wireless communications. *Opt. Wirel. Commun. III* **2001**, *4214*, 26–37. [[CrossRef](#)]
26. Kaymak, Y.; Fathi-Kazerooni, S.; Rojas-Cessa, R.; Feng, J.; Ansari, N.; Zhou, M.; Zhang, T. Beam with Adaptive Divergence Angle in Free-Space Optical Communications for High-Speed Trains. 2018. Available online: <http://arxiv.org/abs/1812.11233> (accessed on 9 June 2022).
27. Taheri, M.; Ansari, N.; Feng, J.; Rojas-Cessa, R.; Zhou, M. Provisioning Internet Access Using FSO in High-Speed Rail Networks. *IEEE Netw.* **2017**, *31*, 96–101. [[CrossRef](#)]
28. Gard, A. Automatic and Manual Barriers. Available online: <https://www.autogard.cz/underwood/download/files/autogard-automatic-and-manual-barriers.pdf> (accessed on 9 June 2022).
29. Gu, J.; Börklü, H.R.; Kalyon, S.A. A Design Study of an Innovative Barrier System for Personal Parking Lots. *J. Sci. Part A Eng. Innov.* **2017**, *4*, 113–123. Available online: <http://dergipark.gov.tr/gujisa> (accessed on 9 June 2022).
30. Kaymak, Y.; Rojas-Cessa, R.; Feng, J.; Ansari, N.; Zhou, M. On Divergence-Angle Efficiency of a Laser Beam in Free-Space Optical Communications for High-Speed Trains. *IEEE Trans. Veh. Technol.* **2017**, *66*, 7677–7687. [[CrossRef](#)]
31. International Electrotechnical Commission (IEC). IEC Standard No. IEC 60825-1:2014. Safety of Laser Products—Part 1: Equipment Classification and Requirements. Available online: <https://webstore.iec.ch/publication/3587> (accessed on 20 August 2022).